

Detection of  ${}^7\text{Be}$  II in the Classical Nova V5669 Sgr (Nova Sagittarii 2015 No.3)

AKIRA ARAI,<sup>1</sup> AKITO TAJITSU,<sup>2</sup> HIDEYO KAWAKITA,<sup>1</sup> AND YOSHIHARU SHINNAKA<sup>1</sup>

<sup>1</sup>*Koyama Astronomical Observatory, Kyoto Sangyo University, Motoyama, Kamigamo, Kita-ku, Kyoto-city, Kyoto, Japan, 803-8555, Japan*

<sup>2</sup>*Subaru Telescope, National Astronomical Observatory of Japan, 650 North A'ohoku Place, Hilo, HI 96720, USA*

## ABSTRACT

We report the new detection of  ${}^7\text{Be}$  II in the ultraviolet spectra of V5669 Sgr during its early decline phase (+24 and +28 d). We identified three blue-shifted absorption systems in our spectra. The first two, referred to as low- and high-velocity components, were noticeably identified among H I Balmer, Na I D, and Fe II whose lower energies of transients are low ( $< 4$  eV). The third absorption component was identified among N II, He I, and C II lines whose lower energy levels are relatively high (9–21 eV). The absorption lines of  ${}^7\text{Be}$  II at 3130.583 Å, and 3132.228 Å were identified as the first and second components in our observations. No evidence suggested the existence of Li I at 6708 Å in any velocity components. The estimated number density ratio of lithium relative to hydrogen, which was finally produced by this object using the equivalent widths of  ${}^7\text{Be}$  and Ca II K,  $N({}^7\text{Li})/N(\text{H})_{\text{final}}$ , is  $4.0 \pm 0.7 \times 10^{-6}$ . This value is an order of magnitude lower than the average observed values for classical novae wherein  ${}^7\text{Be}$  has been detected, and is comparable to the most optimistic value of theoretical predictions.

*Keywords:* nuclear reactions, nucleosynthesis, abundances—stars: individual: Nova Sagittarii 2015 No.3: V5669 Sgr—novae, cataclysmic variables—Galaxy: evolution—techniques: spectroscopic.

## 1. INTRODUCTION

The  ${}^7\text{Li}$  production in classical novae was first confirmed in V339 Del by Tajitsu et al. (2015). They reported the detection of blue-shifted absorption lines of the resonance lines of  ${}^7\text{Be}$  II at 3130.583 Å and 3132.228 Å in near-ultraviolet (UV) high-resolution spectra.  ${}^7\text{Be}$  is an unstable isotope that decays to form  ${}^7\text{Li}$  through the electron capture within a half-life of 53.22 days. Therefore, the detection of  ${}^7\text{Be}$  II lines in the nova spectra provides crucial evidence of  ${}^7\text{Li}$  production by nova explosion. Since the first confirmation of  ${}^7\text{Li}$  production,  ${}^7\text{Be}$  II and/or Li I 6708 Å have been directly detected in several classical novae through high-resolution spectroscopic observations. The first detection of Li I at 6708 Å was reported in V1369 Cen (Izzo et al. 2015). The second and third detections of  ${}^7\text{Be}$  II were reported in V5669 Sgr (Molaro et al. 2016; Tajitsu et al. 2016) and V2944

Oph (Tajitsu et al. 2016), respectively. These three classical novae showed slow declines in their light curves, which suggests that they are CO novae. Furthermore, Izzo et al. (2018) reported  ${}^7\text{Be}$  II detection in a very fast nova V407 Lup. For another very fast nova, V838 Her, Selvelli et al. (2018) reported the existence of absorption and emission features of  ${}^7\text{Be}$  II in the historical UV spectra obtained by *the International Ultraviolet Explorer* (Bogges et al. 1978). The very rapid decline in their light curves (duration up to +2 mag after the maximum,  $t_2 \sim 5$  and 2 d for V407 Lup and V838 Her, respectively) and characteristics of their spectra indicate that they are ONe novae. Recently Molaro et al. (2020) reported further detections of  ${}^7\text{Be}$  II and/or Li I in Nova Mus 2018 and ASASSN-18fv. These two classical novae are probably CO novae because their light curves indicate that they are moderately fast or slow novae. Molaro et al. (2020) summarized that the abundance (number) ratio of  ${}^7\text{Li}$  to hydrogen enhanced by the above-observed novae,  $N({}^7\text{Li})/N(\text{H})$ , is in the range of  $1.5\text{--}17 \times 10^{-5}$  (average of  $5.4 \times 10^{-5}$ ). No major difference exists in the  $N({}^7\text{Li})/N(\text{H})$  ratio among CO and ONe novae. This observational fact implies that  ${}^7\text{Li}$  production widely occurs in classical novae. Using recent observational results, Cescutti & Molaro (2019) demonstrated that Li production in classical novae could mostly explain the Galactic Li evolution curve without remarkable contributions from other source candidates (e.g., red giants and AGB stars).

In studies of  ${}^7\text{Li}$  production in classical novae, theoretical predictions preceded observations. Cameron & Fowler (1971) first established  ${}^7\text{Li}$  production in red giants via the  ${}^3\text{He}(\alpha, \nu){}^7\text{Be}$  reaction, and since then, a number of efforts have been undertaken on thermonuclear runaway (TNR) in classical novae. Arnould & Norgaard (1975) calculated the  ${}^7\text{Li}$  production rate for several combinations of fixed temperatures and densities to study the resulting nucleosynthesis. Starrfield et al. (1978) used their hydrodynamic code to investigate nucleosynthesis during a TNR in a solar-abundance envelope on a white dwarf (WD) and found that  ${}^7\text{Li}$  can be overproduced. José & Hernanz (1998) conducted realistic hydrodynamic calculations that took into account the temperature development in the envelope during the accretion phase before the onset of the TNR and predicted the Li production during the TNR, obtaining values of  $N({}^7\text{Li})/N(\text{H})$  of  $\lesssim 4.7 \times 10^{-6}$  and  $\lesssim 4.8 \times 10^{-6}$  for ONe novae and CO novae, respectively. Several studies on Li evolution in the galaxy that draw on the results of such numerical simulations have concluded that classical novae may contribute up to 10% of the Li produced in the recent universe (Hernanz et al. 1996; Prantzos 2012). Recently, using the Modules for Experiments in Stellar Astrophysics (MESA) code (e.g., Paxton et al. 2011), Rukeya et al. (2017) reported the prediction of  ${}^7\text{Li}$  production similar to those of José & Hernanz (1998). Starrfield et al. (2020) obtained the largest  ${}^7\text{Li}$  production obtained to date for a  $1.35 M_{\odot}$  CO WD [ $N({}^7\text{Be})/N(\text{H}) = 7.0 \times 10^{-6}$ ], assuming that mixing between the core and solar-abundance material in the envelope gas transferred from the companion star switches on immediately after the onset of the TNR. However, such estimates of  $N({}^7\text{Be})/N(\text{H})$  still amount to only several tenths of derived from the observations. José et al. (2020) developed a more realistic model, which incorporates mixing and convection extracted directly from their own 3D simulations back into a 1D model. Their results suggest that the  ${}^7\text{Li}$  production is much less than that obtained in the previous works (e.g., Rukeya et al. 2017 and Starrfield et al. 2020); however, the abundances they obtained for the intermediate-mass elements agree with the observations. In addition to the large disagreement between the observations and the theoretical predictions, large variations exist among the theoretical predictions of the amounts of  ${}^7\text{Li}$  produced. This suggests that the results may depend strongly on differences in the handling of mixing and convection and of the accretion phase before the TNR.

The recent observational facts strongly suggest that classical novae are the major sources of Li in the galaxy. However, some questions on this phenomenon still remain. The first question concerns the discrepancy between the observed abundances and theoretical predictions as described above. The appearance rate of Li production is another question. Recently, [Molaro et al. \(2020\)](#) reported the detection of neither  ${}^7\text{Be}$  II nor Li I in the post-outburst spectra of ASASSN-17hx and Nova Cir 2018. This is the first nondetection report of  ${}^7\text{Be}$  II or Li I in classical novae after [Tajitsu et al. \(2015\)](#), and it suggests that there could be a large scattering of  ${}^7\text{Li}$  production among classical novae. Solving these questions is essential for more precise understandings of the contributions of classical novae to Galactic Li evolution. Therefore, further observations of  ${}^7\text{Be}$  II (and Li I) in classical novae during their early decline phases are required. In this study, we report a new detection of  ${}^7\text{Be}$  II in V5669 Sgr (Nova Sgr 2015 No.3).

## 2. V5669 SGR (NOVA SAGITARII 2015 NO.3)

V5669 Sgr (Nova Sgr 2015 No.3) was discovered as a possible transient object, PNV J18033275-2816054, by Koichi Itagaki on UT 27.429 September 2015 at 9.8 mag (unfiltered) using a 0.5 m Schmidt Cassegrain telescope with an unfiltered CCD camera at his private observatory ([Nakano et al. 2015](#)). The earliest spectroscopic observation by [Fujii \(2015\)](#) with a low-resolution spectrograph ( $R \sim 500$ ) on a 40 cm telescope at the Fujii-Kurosaki Observatory (in Okayama, Japan) was performed around 1.4 h after the discovery, and his spectra show H I Balmer, Fe II and Na I emission lines with P-Cygni profiles, suggesting that the expanding velocity was approximately  $1100 \text{ km s}^{-1}$ . [Williams et al. \(2015\)](#) also reported spectra taken by the FRODOSpec ([Barnsley et al. 2012](#)) on the 2.0 m Liverpool Telescope (in Spain) around 10 h after the discovery, which showed remarkable lines of H I, Fe II, O I  $\lambda 7773$ ,  $\lambda 8446$ , and He I  $\lambda 6678$ . The emission and absorption features of  $\text{H}\alpha$  indicate that the expansion velocity was around  $2000 \text{ km s}^{-1}$ . They concluded that the spectral type ([Williams 1992](#)) of the nova was classified into Fe II class.

**Table 1.** Information of V5669 Sgr.

Item	Value
Discovery date	UT 2015 September 27.4293 MJD 57292.4293
Coordinate (J2000.0)	$\alpha = 18^{\text{h}}03^{\text{m}}32^{\text{s}}.75$ , $\delta = -28^{\circ}16'05''.4$
$t_{\text{max}}$	2015 September 29.1 (MJD 57294.1)
$V_{\text{max}}$	$8.572 \pm 0.001$ mag
$(B - V)_{\text{max}}$	$0.793 \pm 0.001$ mag
$t_2$	24 days
$E_{B-V}^*$	$0.44 \pm 0.02$ mag
$M_V^*$	$-7.8 \pm 0.4$ mag
$d^*$	$10.0 \pm 1.9$ kpc

NOTE—\*: The estimation of the interstellar extinction ( $E_{B-V}$ ), the absolute magnitudes ( $M_V$ ), and the distance ( $d$ ) are shown in Appendix A.

**Table 2.** Journal of Observations of V5669 Sgr by Subaru/HDS

Date	MJD	t (day)	Seup	Exp. time (sec)	Airmass
23 Oct 2015	57318.19	+24.09	Ub	3000	1.88
23 Oct 2015	57318.23	+24.13	Yb	1800	2.58
27 Oct 2015	57322.19	+28.09	Ub	2400	1.97
27 Oct 2015	57322.22	+28.12	Yb	1800	2.59

Figure 1 displays the optical light curves of V5669 Sgr<sup>1</sup>. The object was discovered during the early rising phase about 1.6 d before the maximum. We set the first maximum date to MJD 57294.1 ( $= t_0$ ) at  $V = 8.57$  mag based on data in the Stony Brook/SMARTS Atlas. The basic parameters of the nova are listed in Table 1. The estimations of the extinction,  $E_{B-V}$ , the absolute magnitude,  $M_V$ , and the distance,  $d$ , are shown in Appendix A using the SMARTS data set and measurements of diffuse interstellar bands detected in our high-resolution spectra.

V5669 Sgr is potentially a CO nova as it shows a moderately fast decline in its brightness with  $t_2 = 24$  d. Strong Fe II, Na I, or O I lines associated with the P-Cygni profile are dominant in the initial spectra described above and also in our spectra (see Section 4). Note that He/N-type emission features, which are often observed in early decline phases of ONe novae, are not prominent among them.

After its explosion, V5669 Sgr was detected in the GAIA DR2 catalog as a source of  $G = 14.3$  (GAIA DR2 4062508582302805760) 0.16 arcsec apart from the position of the nova. Its parallax and distance are not available in the catalog. Moreover, no counterparts are present in the Pan-STARRS catalog (Chambers et al. 2016). The nearest red star in the Pan-STARRS catalog was found at 0.9 arcsec apart from the nova (PSO J180332.784-281604.706,  $g = 19.02 \pm 0.04$ ,  $r = 18.102 \pm 0.003$ ), whose counterpart can be found in the GAIA DR2 catalog (GAIA DR2 4062508582302826240,  $G = 18.25$ ). Thus, we concluded that the progenitor is not detected in the Pan-STARRS and previous surveys.

### 3. OBSERVATIONS AND REDUCTIONS

We performed optical high dispersion spectroscopic observations for V5669 Sgr using the High Dispersion Spectrograph (HDS; Noguchi et al. 2002) mounted on the 8.2 m Subaru telescope and succeeded at two epochs (+24 and +28 d) during its rapid decline phase. Table 2 shows a summary of our HDS observations. Our spectra cover 3020–6865 Å with two different grating settings of the spectrograph: Setup-Ub, 3020–4631 Å with a gap at 3748–3790 Å, and Setup-Yb, 4108–6865 Å with a gap at 5434–5514 Å. The spectral resolving power was  $\sim 45,000$  with a 0.80" (0.4 mm) slit width. Data reduction was conducted using the Image Reduction and Analysis Facility (IRAF)<sup>2</sup> software with the standard manner for HDS data<sup>3</sup>. The non-linearity of the CCD pixels was corrected using the

<sup>1</sup> Photometric data are taken from Nakano et al. (2015) the AAVSO Archives (Kafka, S., 2019, Observations from the AAVSO International Database, <https://www.aavso.org>), and The Stony Brook/SMARTS Atlas of Southern Novae (<http://www.astro.sunysb.edu/fwalter/SMARTS/NovaAtlas/atlas.html> Walter et al. 2012).

<sup>2</sup> IRAF is distributed by the National Optical Astronomy Observatory, which is operated by the Association of Universities for Research in Astronomy (AURA) under a cooperative agreement with the National Science Foundation.

<sup>3</sup> <https://www.naoj.org/Observing/Instruments/HDS/hdsq-e.html>

**Table 3.** List of Identified Emission Lines in Figure 2.  $\lambda_{\text{obs}}$  is the observed wavelength around the center of each emission line on +24 d.  $\lambda_{\text{rest}}$  is the laboratory wavelength. The multiplet numbers are taken from Moore (1972). The left curly brackets denote the observed blended lines in the column between  $\lambda_{\text{rest}}$  and  $\lambda_{\text{lab}}$ .

$\lambda_{\text{obs}}(\text{\AA})$	$\lambda_{\text{lab}}(\text{\AA})$	Line	$\lambda_{\text{obs}}(\text{\AA})$	$\lambda_{\text{lab}}(\text{\AA})$	Line
3794.2	3797.909	H $\theta$	4864.6	4861.350	H $\beta$
3835.3	3835.397	H $\eta$	4926.0	4923.921	Fe II (42)
3888.1	3889.064	H $\zeta$	5022.0	5018.436	Fe II (42)
3930.4	3933.68	Ca II K	5173.0	5169.028	Fe II (42)
3972.5	3968.66	Ca II H	5278.2	5275.997	Fe II (49)
	+3970.075	H $\epsilon$	5320.7	5316.609	Fe II (49)
4102.5	4101.734	H $\delta$	5749.1	5747.300	N II (9)
4125.1	4122.638	Fe II (28)	5894.3	5892.937	Na I D
4177.6	4173.450	Fe II (27)	6152.1	6149.246	Fe II (74)
4239.5	4233.160	Fe II (27)	6303.0	6300.304	[O I]
4350.6	4340.472	H $\gamma$	6361.3	6363.776	[O I]
	+4351.763	Fe II (27)	6567.9	6562.79	H $\alpha$
4473.4	4471.48	He I			

method described by Tajitsu et al. (2010). The wavelength calibration was performed using the Th-Ar comparison spectra. The typical residual in the wavelength calibration was approximately  $10^{-3}$   $\text{\AA}$  ( $\sim 0.1$   $\text{km s}^{-1}$ ). The observed spectra were converted to the heliocentric wavelength scale. Spectrophotometric calibrations were performed with the spectra of  $\sigma$  Sgr ( $V = 2.058$ , B2V<sup>4</sup>) obtained nearly at the same airmass of the nova on the same nights. The telluric absorption correction was not performed.

In principle, we refer to Kramida et al. (2019) for wavelengths,  $\log(gf)$ s, and lower and upper transition energies ( $E_{\text{low}}$  and  $E_{\text{up}}$ ) of each ion herein. Multiplet numbers are taken from Moore (1972). We refer to such parameters of Cr II (5) lines from Nilsson et al. (2006).

## 4. RESULTS

### 4.1. Overview

Figure 2 shows the overall spectra of V5669 Sgr obtained on +24 and +28 d. The identifications of strong emission lines are listed in Table 3. The emission lines originating from the H I Balmer series, Fe II, and Ca II are easily identified in the spectra. These strong emission lines are accompanied by P-Cygni-like profiles, and the mean FWHMs of these emission lines are approximately  $2000$   $\text{km s}^{-1}$ . Each H I emission line has a saddle-shaped profile, as seen in the H $\alpha$  emission line shown in the inset in the panel of Figure 2. These spectral features indicate that the nova is an ordinary Fe II-type classical nova with a CO WD as reported in previous studies (Fujii 2015; Williams et al. 2015).

<sup>4</sup> These values are taken from Simbad (Wenger et al. 2000).

#### 4.2. *Blueshifted Absorption Line Systems (Low- and High-Velocity Components)*

Figure 3 displays the enlarged views of the spectra taken on +24 d (left) and +28 d (right) in the vicinities of  $H\gamma$ , Ca II K, Fe II (42)  $\lambda 5169.03$ , Na I D<sub>2</sub>, and  ${}^7\text{Be II } \lambda 3131.228$ . Two blue-shifted absorption components accompany each of the first three lines in both epochs. Hereafter, we refer to them as the low-velocity component (LVC) and high-velocity component (HVC). On +24 d, the LVC ( $v_{\text{rad}} = -840$  to  $-1260$  km s<sup>-1</sup>) and HVC ( $v_{\text{rad}} = -1800$  to  $-2200$  km s<sup>-1</sup>) are very distinct. Until +28 d, the HVC definitely accelerated to  $v_{\text{rad}} = -1850$  to  $-2500$  km s<sup>-1</sup>. The LVC had a somewhat mild acceleration to  $v_{\text{rad}} = -840$  to  $-1300$  km s<sup>-1</sup>. Moreover, LVC and HVC of Na I D, and  ${}^7\text{Be II}$  can be identified in both epochs, although some contaminations arising from other metal lines are expected. The strengths of most blue-shifted absorption lines became weaker from +24 to +28 d. The decrease in the equivalent width ( $W$ ),  $\Delta W = -0.88 \pm 0.07$  Å for the LVC, and  $-2.73 \pm 0.06$  Å for the HVC, is observed clearly for Fe II  $\lambda 5169.028$  ( $E_{\text{low}} = 2.89$  eV). The similar blueshifted absorption line systems are occasionally observed in previous novae, for example, V2659 Cyg (Arai et al. 2016). As in V2659 Cyg, numerous absorption lines can be identified with LVC originating from singly ionized Fe-peak elements (Ti II, Cr II, and Mn II). Most of them do not accompany their emission lines. They are essentially the same as the “transient heavy element absorption (THEA)”, proposed and discussed in Williams et al. (2008).

#### 4.3. *Another Blueshifted Absorption System (Third Velocity Component)*

Figure 4 shows representative spectra in the vicinities of N II (3)  $\lambda 5666.63$  and He I  $\lambda 5875.621$ ,  $\lambda 6678.151$  on +24 and +28 d. Absorption lines accompanied by these lines are identified as a single component. On +24 d, the velocity range of this component,  $v_{\text{rad}} = -1450$  to  $-2070$  km s<sup>-1</sup>, is similar to that of HVC in this epoch. On +28 d, however, the component accelerated up to  $-2100$  to  $-2650$  km s<sup>-1</sup>, which is different from the velocities of both LVC and HVC in this epoch. The absorption lines of this component have somewhat smooth, round-shaped profiles compared with those in LVC and HVC displayed in Figure 3. This absorption system is not accompanied by any emission lines except for N II (3)  $\lambda 5666.63$  ( $E_{\text{low}} = 18.47$  eV) and He I  $\lambda 5875.621$  blending with Na I D. Several N II lines (e.g.,  $\lambda 5747.30$ ) have absorption lines corresponding to this system. The  $E_{\text{low}}$  of these lines is in the range of 9.3–21 eV, which is significantly higher than that in the LVC and HVC systems reported in Section 4.2. Considering these characteristics, we conclude that this blue-shifted absorption component is the third component that is neither LVC nor HVC. Hereafter we name it the third velocity component (TVC) for convenience. We note that the TVC in V5669 Sgr is similar to the absorption components of N II and He I identified in V407 Lup (Izzo et al. 2018). In V407 Lup, the radial velocity of this velocity component reached  $-3830$  km s<sup>-1</sup> in contrast to the low velocities of Fe II and H I lines ( $\sim -2300$  km s<sup>-1</sup>).

#### 4.4. *${}^7\text{Be II}$ Abundance*

As shown in Figure 3, we can identify absorption lines belonging to the LVC and HVC systems of  ${}^7\text{Be II}$  for the spectra on both +24 and +28 d. Following the previous studies of  ${}^7\text{Be II}$  (Tajitsu et al. 2015, 2016), the  ${}^7\text{Be}$  abundance in the LVC and HVC can be estimated by the ratios of  $W$ s between  ${}^7\text{Be II } \lambda\lambda 3131$  and Ca II K lines.

Prior to our abundance estimations, we evaluated contaminations from other metal lines to the  $W$ s of  ${}^7\text{Be II } \lambda\lambda 3131$ . No remarkable contamination was expected for Ca II K, because no strong lines originated from Fe-peak ions around it. The complicated profiles of the LVC and HVC of  ${}^7\text{Be II}$

**Table 4.** Candidates of Lines Contaminating  ${}^7\text{Be}$  II.

Line	Rest wavelength( $\text{\AA}$ )	$\log(gf)^*$	$W(\text{\AA})^\dagger$	Contamination
Cr II (5)	3118.649	-0.102	<i>0.24</i>	HVC
Cr II (5)	3120.369	+0.108	<i>0.38</i>	HVC
Cr II (5)	3124.978	+0.286	$0.55 \pm 0.02$	
Cr II (5)	3128.700	-0.528	<i>0.09</i>	LVC
Cr II (5)	3132.056	+0.437	<i>0.82</i>	LVC

NOTE— \*: All  $\log(gf)$  values of Cr II (5) lines are quoted from Nilsson et al. (2006).

†: Measured equivalent widths is only for Cr II  $\lambda$ 3124.978.  $W$ s for other lines (italic letters) are calculated using their  $\log(gf)$  values.

We regarded that Cr II (5)  $\lambda$ 3128.700 contaminates  ${}^7\text{Be}$  II with half of its  $W$  [ $= 0.5 \times W_\lambda(\text{Cr II } \lambda 3128.700)$ ].

indicated that  ${}^7\text{Be}$  II is contaminated with some absorption lines originating from Cr II (5), Fe II (82), and Ti II (67), as mentioned in the previous studies (Tajitsu et al. 2016; Molaro et al. 2016, 2020). In our spectra of V5669 Sgr, the HVC of Fe-peak elements (Fe II, Ti II, Cr II and Mn II) are generally very faint or unidentified except for strong Fe II lines (e.g., Fe II  $\lambda$ 5018.436 and  $\lambda$ 5169.028). We consider that the LVCs of Fe-peak elements are the dominant source of contamination for  ${}^7\text{Be}$  II lines. In the vicinity of  ${}^7\text{Be}$  II on +24 d, distinguishing each contaminating line is difficult due to the heavy blending of  ${}^7\text{Be}$  II  $\lambda$ 3131 and lines of Fe-peak elements. As we reported in Section 4.2, the LVC and HVC of Fe-peak elements (Fe II, Ti II, Cr II and Mn II) on +28 d are weaker than those on +24 d. Therefore, hereafter, we estimate the  ${}^7\text{Be}$  abundance using the spectrum on +28 d. In the spectrum on +28 d, we can identify the unblended LVC of Cr II (5)  $\lambda$ 3124.978 [ $E_{\text{low}} = 2.45$  eV,  $E_{\text{per}} = 6.42$  eV,  $\log(gf) = 0.286$ ], whose  $W$  is  $0.55 \pm 0.02$   $\text{\AA}$ , which is between the LVC and HVC of  ${}^7\text{Be}$  II (Figure 3). Other candidates of the contaminating lines originating from Fe-peak elements in this region are Fe II (82) ( $E_{\text{low}} = 3.9$  eV,  $E_{\text{up}} = 7.8$  eV) at 3135.36  $\text{\AA}$  [ $\log(gf) = -1.13$ ], 3144.75  $\text{\AA}$  (-1.74) as shown in Table 2 in Molaro et al. (2016), and Ti II (67) ( $E_{\text{low}} = 1.2$  eV,  $E_{\text{up}} = 5.2$  eV), 3106.25  $\text{\AA}$  (-0.17), 3117.68  $\text{\AA}$  (-0.50), 3119.83  $\text{\AA}$  (-0.46) as shown in Table 2 in Tajitsu et al. (2016). Their  $\log(gf)$  values are smaller than those of Cr II (5) [ $\log(gf) = -0.102 - +0.437$ ]. Furthermore, we identify no significant lines originated from Fe II (82) and Ti II (67) on +28 d even in the wavelength region free from the LVC and HVC of  ${}^7\text{Be}$  II. Therefore, we ignored contaminations from these multiplet lines. We estimated  $W$ s of nearby Cr II (5) lines using their  $\log(gf)$  values and the measured  $W$  of Cr II (5)  $\lambda$ 3124.978. The estimated  $W$ s of other Cr II (5) lines are summarized in Table 4 with the absorption components of  ${}^7\text{Be}$  II (LVC or HVC) that they may contaminate. The total  $W$ s of Cr II (5) contaminating  ${}^7\text{Be}$  II is  $0.87 \pm 0.02$   $\text{\AA}$  for the LVC and  $0.59 \pm 0.03$   $\text{\AA}$  for the HVC.

The measured  $W$ s of  ${}^7\text{Be}$  II in the spectrum on +28 d are  $1.58 \pm 0.02$   $\text{\AA}$  for the LVC and  $1.22 \pm 0.02$   $\text{\AA}$  for the HVC. After excluding the contamination from Cr II (5) lines, we obtained the intrinsic  $W$ s of  ${}^7\text{Be}$  II as  $0.76 \pm 0.06$   $\text{\AA}$  for LVC and  $0.63 \pm 0.07$   $\text{\AA}$  for HVC. The measured  $W$ s of Ca II K, which have no contaminations, are  $1.63 \pm 0.03$   $\text{\AA}$  for the LVC and  $0.73 \pm 0.03$   $\text{\AA}$  for the HVC. Using these  $W$ s of  ${}^7\text{Be}$  II and Ca II K in Equation (1) in Tajitsu et al. (2016), the number density ratios of

$N(^7\text{Be})/N(\text{Ca})$ , was calculated. We relied on the same three assumptions as in Tajitsu et al. (2015) and other previous studies. Those are (1) the difference in the color of the background light at 3131 Å and 3930 Å can be ignored, (2) all  $^7\text{Be}$  and Ca in the nova ejecta are in their singly ionized states, and (3) the  $N(\text{Ca})/N(\text{H})$  in the absorbing gas cloud is the solar value. Consequently, we obtained the total number density ratio,  $N(^7\text{Be})/N(\text{Ca}) = 1.01 \pm 0.09$ , and  $1.87 \pm 0.21$  for the LVC and HVC, respectively. If we assume that  $N(\text{Ca})/N(\text{H})$  in the absorbing gas is the same as that of the solar photosphere ( $2.19 \times 10^{-6}$ ; Asplund et al. 2009), we obtain  $N(^7\text{Be})/N(\text{H}) = 2.2 \pm 0.2 \times 10^{-6}$  and  $4.1 \pm 0.5 \times 10^{-6}$  for the LVC and HVC, respectively. This  $N(^7\text{Be})/N(\text{H})$  can be converted into the mass ratio,  $X(^7\text{Be})/X(\text{H}) = 1.5 \pm 0.1 \times 10^{-5}$  and  $2.9 \pm 0.3 \times 10^{-5}$  for the LVC and HVC, respectively.

In addition to the effects from line contaminations, which we have discussed above, our three assumptions adopted in this  $N(^7\text{Be})/N(\text{H})$  estimation may cause uncertainties in the results. We expect that the most significant uncertainty originates from the difference in the color of the background light in the range of  $^7\text{Be}$  II or Ca II; this is mainly caused by the overlap of the broad emission lines with the background continuum. By polynomial function fitting, we found that the amplitudes of the undulated continuum level are  $\sim 25\%$  in the nearby region of  $^7\text{Be}$  II (3080Å–3140Å). This directly corresponds to a  $\pm 25\%$  error in the measured  $W$ , i.e., the estimated  $N(^7\text{Be})/N(\text{H})$ . Regarding the second assumption, the ionization potential is a little different between  $^7\text{Be}$  II (the first and second ionization potentials;  $I_1 = 9.32$ ,  $I_2 = 18.21$  eV) and Ca II ( $I_1 = 6.11$  eV and  $I_2 = 11.87$  eV; Kramida et al. 2019). Some singly ionized iron-peak elements (Ti to Fe) are found in the LVC absorption system in V5669 Sgr (see Section 4.2). Their ionization potentials are between those of Be and Ca ( $I_1=6.8\text{--}7.9$  eV,  $I_2 = 3.6\text{--}18.1$  eV). This situation is quite similar to that in V339 Del (Tajitsu et al. 2015). Therefore, we expected that the large fractions of Be and Ca are in the singly ionized states, as also in the case of V5669 Sgr on  $t = 28$  d. Considering the third assumption,  $N(\text{Ca})/N(\text{H})$ s in nova yields tend to be comparable to or even higher than the solar value up to  $\sim 10\%$ – $20\%$  in some theoretical simulations for CO novae (e.g., José et al. 2020) in which the gas with solar abundance is assumed to accumulate on the surface of the WD. It is mainly caused by the consumption of hydrogen during TNR. If we adopt this hydrogen reduction in TNR, the  $N(^7\text{Be})/N(\text{H})$  of V5669 Sgr can be underestimated up to  $10\%$ – $20\%$ . Finally, the total error caused by our assumptions is  $-25\%$ – $+50\%$  for  $N(^7\text{Be})/N(\text{H})$  in Table 5.

All  $^7\text{Be}$  eventually decays to  $^7\text{Li}$  through the reaction of  $^7\text{Be}(e^-, \nu_e)^7\text{Li}$  with a half-life,  $\tau_{1/2} \sim 53$  days. Therefore the total number of  $^7\text{Be}$  isotopes produced in the TNR,  $N(^7\text{Be})_{\text{TNR}}$ , must be equal to the final  $^7\text{Li}$  produced in the observed outburst,  $N(^7\text{Li})_{\text{final}}$ .  $N(^7\text{Li})_{\text{final}}$  can be estimated using  $N(^7\text{Be})_{\text{TNR}} = N(^7\text{Li})_{\text{final}} = 2^{t/\tau_{1/2}} \times N(^7\text{Be}, t_{\text{obs}})$ , where  $t_{\text{obs}} = +28$  d. The final  $^7\text{Li}$  abundance produced by V5669 Sgr is expected to be  $N(^7\text{Li})/N(\text{H})_{\text{final}} = 3.17 \pm 0.27 \times 10^{-6}$  for the LVC and  $5.88 \pm 0.66 \times 10^{-6}$  for the HVC. Here, we use  $W(\text{Ca II K})$ s for the LVC and HVC as the weight for mass ratios between them, then get a weighted  $N(^7\text{Li})/N(\text{H})_{\text{final}}$  for the nova as  $4.0 \pm 0.7 \times 10^{-6}$ . We will use this averaged  $N(^7\text{Li})/N(\text{H})_{\text{final}}$  in our discussion hereafter, which corresponds to the mass ratio of  $X(^7\text{Li})/X(\text{H})_{\text{final}} = 2.8 \pm 0.5 \times 10^{-5}$ .

Our results of  $^7\text{Be}$  abundance estimation are summarized in Table 5. The  $N(^7\text{Li})/N(\text{H})_{\text{final}}$  observed in V5669 Sgr is smaller by a factor of 13.5 than the mean value in previous studies of other observed novae ( $5.4 \times 10^{-5}$ ; Molaro et al. 2020). It is still 3–5 dex larger than the  $^7\text{Li}$  meteoritic value ( $N(^7\text{Li})/N(\text{H}) = 1.86 \times 10^{-9}$ ), and significantly larger than the solar photospheric value ( $1.12 \times 10^{-11}$ ) given in Asplund et al. (2009). It is rather comparable to the upper limit of numerical predictions



**Table 5.** Equivalent Widths and Observed Abundances of  ${}^7\text{Be}$  in V5669 Sgr.

	$W({}^7\text{Be II})$ ( $\text{\AA}$ )	$W(\text{Ca II K})$ ( $\text{\AA}$ )	$\frac{N({}^7\text{Be})}{N(\text{Ca})}$	$\frac{N({}^7\text{Be})}{N(\text{H})}$ ( $10^{-6}$ )	$\frac{N({}^7\text{Li})}{N(\text{H})_{\text{final}}}$ ( $10^{-6}$ )	$\frac{X({}^7\text{Li})}{X(\text{H})_{\text{final}}}$ ( $10^{-5}$ )
LVC	$0.76 \pm 0.06$	$1.63 \pm 0.03$	$1.01 \pm 0.09$	$2.2 \pm 0.2$	$3.17 \pm 0.27$	$2.23 \pm 0.19$
HVC	$0.63 \pm 0.07$	$0.73 \pm 0.03$	$1.87 \pm 0.21$	$4.1 \pm 0.5$	$5.88 \pm 0.66$	$4.12 \pm 0.46$

for CO novae by [José & Hernanz \(1998\)](#) ( $4.8 \times 10^{-6}$ ) and [Starrfield et al. \(2020\)](#) ( $7.0 \times 10^{-6}$ ). We compare this result in V5669 Sgr with previous studies and discuss it in Section 5.

#### 4.5. Absence of Li I

We also checked the resonance doublet of Li I at  $6708 \text{\AA}$  although it has not been detected in most novae. Figure 5 displays the spectra on +24 and +28 d around  $6683 \text{\AA}$ , where the LVC and HVC of Li I  $\lambda\lambda 6708$  are possibly located. On +24 d, a dip at  $6683 \text{\AA}$  is observed. The position of this dip may correspond to that of LVC of Li I  $\lambda\lambda 6708$  ( $v_{\text{rad}} \sim 1000 \text{ km s}^{-1}$ ). It may also agree well with the TVC of C II  $\lambda 6723.32$  [ $\log(gf) = -1.156$ ,  $E_{\text{low}} = 20.84 \text{ eV}$ ,  $E_{\text{up}} = 22.68 \text{ eV}$ ]. The profile of the dip is round-shaped, which conforms to the characteristics of the TVC (Section 4.3). Furthermore, a deep and broad depression around  $6750 \text{\AA}$  is considered to be a blending TVC arising from C II (14) multiplet lines ( $E_{\text{low}} = 20.70$ ,  $E_{\text{up}} = 22.53$ ), at  $6779.94 \text{\AA}$  [ $\log(gf) = +0.03$ ],  $6780.59 \text{\AA}$  ( $-0.38$ ),  $6783.91 \text{\AA}$  ( $+0.30$ ),  $6787.21 \text{\AA}$  ( $-0.38$ ), and  $6791.47 \text{\AA}$  ( $-0.27$ ). Since the  $E_{\text{low}}$  of C II (14) and C II  $\lambda 6723.32$  are very close, the latter's absorption strength can be estimated using that of the former by referring to their  $\log(gf)$  values. The measured  $W$  of the blending TVC of C II (14),  $6.3 \text{\AA}$ , raises the expectation that the  $W$  of C II  $\lambda 6723.32$  should be  $\sim 0.1 \text{\AA}$ . The measured  $W$  of the dip at  $6683 \text{\AA}$ ,  $\sim 0.21 \pm 0.03 \text{\AA}$ , is slightly larger than this value. The discrepancy between them can be explained by the saturation effect of C II (14) multiplet lines as the  $\log(gf)$  values of most multiplets in C II (14) are much larger than that of C II  $\lambda 6723.32$ .

On +28 d, there are no noteworthy dips in the range of  $6679\text{--}6689 \text{\AA}$ , where the LVC ( $v_{\text{rad}} = -840$  to  $-1300 \text{ km s}^{-1}$ ) of Li I  $\lambda\lambda 6708$  should be located. The TVCs ( $v_{\text{rad}} = -2100$  to  $-2650 \text{ km s}^{-1}$ ) of C II  $\lambda 6723.32$  and C II (14) multiplet should locate at  $\sim 6671 \text{\AA}$  and  $6695 \text{\AA}$ , respectively. However, both of them almost disappeared in this epoch.

In the case of two novae, V1369 Cen ([Izzo et al. 2015](#)) and ASASSN-18fv ([Molaro et al. 2020](#)), in which the Li I  $\lambda\lambda 6708$  absorption line has been detected, the resonance absorption line of Ca I  $\lambda 4226.73$  [ $\log(gf) = 0.244$ ] has been identified with Li I  $\lambda\lambda 6708$  being in the very early stages of their outbursts (at +7–+18 d and 1 d, respectively). Figure 6 shows the spectra of V5669 Sgr in the vicinity of Li I  $\lambda\lambda 6708$  and Ca I  $\lambda 4226.73$ . We found no counterparts of the LVC and HVC of Ca I  $\lambda 4226.73$  in both epochs. Based on these results, we conclude that the absorption of Li I  $\lambda\lambda 6708$  is absent in our spectra of V5669 Sgr in both epochs. We consider that the dip at  $\sim 6683 \text{\AA}$  in the spectrum on +24 d plausibly originates from C II  $\lambda 6723.32$  instead of Li I  $\lambda\lambda 6708$ . The absence of Li I  $\lambda\lambda 6708$  and Ca I  $\lambda 4226.73$  suggests that the excitation degree of ejecta observed as blue-shifted absorption components in V5669 Sgr was high enough to ionize these atoms. This is consistent with our assumption used for our  ${}^7\text{Be}$  abundance estimation in Section 4.4.

**Table 6.** List of  ${}^7\text{Be}$  II and Li I Detected Novae.

Object	$t_2$	$t_{\text{obs}}$	$V_{\text{max}}$	$M_{\text{WD}}$	WD Type	$N({}^7\text{Li})/N(\text{H})_{\text{final}}$
		(d)	( $\text{km s}^{-1}$ )	( $M_{\odot}$ )		( $\times 10^{-5}$ )
<b>V5669 Sgr<sup>(a)</sup></b>	<b>24</b>	<b>28</b>	<b>2900</b>	<b>0.85–1.1</b>	<b>CO</b>	<b>0.40</b>
V339 Del <sup>(b)</sup>	10	47	2700	$1.04 \pm 0.02^{(i)}$	CO	$\sim 2.6$
V5668 Sgr <sup>(d,e)</sup>	60	58, 82	2300	$0.85^{(j)}$	CO	$\sim 15$
V407 Lup <sup>(f)</sup>	5	8	3830	0.85–1.35	ONe	6.2
V2944 Oph <sup>(d)</sup>	–	80	2000	$0.85^{(k)}$	CO	1.6
V838 Her <sup>(g)</sup>	2	1, 3, 4	3500	$1.35^{(j)}$	ONe	2.5
Nova Mus 2018 <sup>(h)</sup>	$\sim 30$	35	2240	0.6–1.1	CO?	1.5
ASASSN-18fv <sup>(h)</sup>	$\sim 45$	80	880	0.6–1.1	CO?	2.2
<i>V1369 Cen<sup>(c,l)</sup></i>	<i>40</i>	<i>7</i>	<i>2500</i>	<i>0.9<sup>(j)</sup></i>	<i>CO</i>	<i>0.015</i>

NOTE— Values of  $N({}^7\text{Li})/N(\text{H})_{\text{final}}$  for all previous reported nova are quoted from Molaro et al. (2020), and averaged values are displayed regarding those of V339 Del and V5668 Sgr.

References:

(a) This study.

(b) Tajitsu et al. (2015).

(c) Izzo et al. (2015).

(d) Tajitsu et al. (2016).

(e) Molaro et al. (2016).

(f) Izzo et al. (2018).

(g) Selvelli et al. (2018).

(h) Molaro et al. (2020).

(i) Chochol et al. (2015).

(j) Hachisu & Kato (2019).

(k) Kato et al. (2009).

(l) We exclude the Li abundance of V1369 Cen in our discussion because it may not reflect the  $N({}^7\text{Li})/N(\text{H})_{\text{final}}$  synthesized in this nova event, as mentioned in Section 5.

## 5. DISCUSSION

V5669 Sgr is the eighth classical nova whose  ${}^7\text{Be}$  abundance has been measured. In addition to V1369 Cen whose  ${}^7\text{Li}$  abundance was directly measured, we summarized  ${}^7\text{Li}$  abundances of nine novae with their physical parameters in Table 6. Considering the decline speed of light curves and WD masses in classical novae, we can roughly guess the WD mass of V5669 Sgr by comparing the  $t_2$  of  ${}^7\text{Be}$  detected novae and their WD masses reported in previous studies. We consider that the WD mass of V5669 Sgr ( $t_2 = 24$  d) is larger than  $0.85 M_{\odot}$  because the WD mass of V5668 Sgr ( $t_2 = 40$  d) is estimated as  $0.85 M_{\odot}$  (Hachisu & Kato 2019). We also consider that the upper limit WD of V5669 Sgr is  $1.1 M_{\odot}$ , which is the highest mass of ordinary CO WD (Althaus et al. 2010). WD masses,  $t_2$ , and  $V_{\text{max}}$  of other novae are quoted from literature, as shown in the caption of Table 6. WD masses of 407 Lup, Nova Mus 2018 and ASASSN-18fv have not yet determined. However, we can roughly estimate ranges of WD mass based on their light-curve characteristics, regardless of whether they

are slow or fast novae. WD masses for three novae are also present in Table 6,  $0.85\text{--}1.35 M_{\odot}$  for 407 Lup, and  $0.6\text{--}1.1 M_{\odot}$  for Nova Mus 2018 and ASASSN-18fv. The measured  $N({}^7\text{Li})/N(\text{H})_{\text{final}}$ s produced by each nova event, which should be equal to  $N({}^7\text{Be})/N(\text{H})_{\text{TNR}}$  values, are in the range of  $0.45\text{--}15 \times 10^{-5}$ . The maximum  $N({}^7\text{Li})/N(\text{H})_{\text{final}}$  is observed for V5668 Sgr, and the lowest one is observed for V5669 Sgr. The  $N({}^7\text{Li})/N(\text{H})_{\text{final}}$  of V1369 Cen, which is also the lowest on the list, is measured by the comparison of Li I  $\lambda\lambda 6708$  with Na ID and K I  $\lambda 7699$  absorption lines, as in [Izzo et al. \(2015\)](#). The ionization state of ejecta in V1369 Cen when Li I is detected ( $t = 7$  d) should be lower than that of  ${}^7\text{Be}$  II detected novae as described in Section 4.4. However, Li (the first ionization potential, 5.39 eV) should be partially ionized in the nova ejecta because Fe (7.87 eV) and Cr (6.77 eV) have been observed in the same absorption component. Due to a lack of  ${}^7\text{Be}$  II observations, the measured Li abundance may not reflect the  $N({}^7\text{Li})/N(\text{H})_{\text{final}}$  synthesized in this nova event. Therefore, we exclude the Li abundance of V1369 Cen in the following discussion.

Here, we compare the observed  $N({}^7\text{Li})/N(\text{H})_{\text{final}}$  with those of the theoretical simulations. Because WD masses are one of the key parameters in TNR simulations, resultant yields are often demonstrated as their functions. In Figure 7, the  $N({}^7\text{Li})/N(\text{H})_{\text{final}}$ s observed in the nine novae are plotted with their estimated WD mass over the results from several theoretical simulations ([José & Hernanz 1998](#); [José et al. 2020](#); [Starrfield et al. 2020](#)). Though the errors of estimated WD masses for the observed novae in Table 6 may be quite huge, it is remarkable that all the observed  $N({}^7\text{Li})/N(\text{H})_{\text{final}}$ s are higher than the results of the theoretical simulations in Figure 7. As we discussed, the error in our  $N({}^7\text{Li})/N(\text{H})_{\text{final}}$  in V5669 Sgr is  $\sim \pm 0.1 \times 10^{-5}$ . The scattering of all the observed  $N({}^7\text{Li})/N(\text{H})_{\text{final}}$ s is considerably large ( $\sim 15 \times 10^{-5}$ ) compared to such errors. This means that the  ${}^7\text{Li}$  productivity must vary in each nova. The  $N({}^7\text{Li})/N(\text{H})_{\text{final}}$  of V5669 Sgr is the lowest among the observed novae and comparable to the upper limit of the theoretical estimations with the WD mass in the range of  $0.85\text{--}1.1 M_{\odot}$  ([José & Hernanz 1998](#); [Starrfield et al. 2020](#)). The discrepancy in the  ${}^7\text{Li}$  yields between the observations and theoretical simulations should still be discussed in future investigations. Furthermore, the  ${}^7\text{Li}$  productivity varies greatly among each existing theoretical simulation. These imply that some additional physical mechanisms need to be considered in theoretical simulations. Moreover, further observational studies are required to understand the variance of Li production in classical novae. [Molaro et al. \(2020\)](#) reported about two novae without  ${}^7\text{Li}$  production. Therefore, pursuing the appearance rate of  ${}^7\text{Li}$  production is quite important as well.

In this paper, we estimated the  ${}^7\text{Li}$  abundance of V5669 Sgr, which is the lowest value among other  ${}^7\text{Be}$  detected novae. Moreover, the value agrees with theoretical predictions of the WD mass range of  $0.85\text{--}1.1 M_{\odot}$ , which is an order of magnitude less than those of previous observations. Our result indicates that there is a scattering in  ${}^7\text{Li}$  production among classical novae as shown in [Molaro et al. \(2020\)](#) who reported a nondetection of  ${}^7\text{Be}$  II lines and very low abundances of  ${}^7\text{Li}$  in two novae. Further observational studies for the  ${}^7\text{Li}$  abundances in classical novae are required to resolve the scattering of  ${}^7\text{Li}$  production among them. This must be key to more precisely understanding the Galactic Li evolution.

This study is based on data collected at the Subaru Telescope, which is operated by the National Astronomical Observatory of Japan. We are honored and grateful for the opportunity of observing the Universe from Maunakea, which has the cultural, historical and natural significance in Hawaii.

We gratefully thank the collaborators of our proposal for observations by the Subaru telescope, Dr. Kozo Sadakane (Osaka Kyoiku University), Dr. Hiroyuki Naito (Nayoro Observatory), Dr. Wako Aoki (National Astronomical Observatory of Japan), Dr. Satoshi Honda (Nishi-Harima Astronomical Observatory, University of Hyogo), and Mr. Mitsugu Fujii (Fujii-Kurosaki Observatory). We are also grateful for the variable star observations from the AAVSO International Database contributed by observers worldwide and that were used in this study. This study is supported by KAKENHI (Grant-in-Aid for Challenging Exploratory Research, 15K13466 and for Scientific Research (C) 19K03933) from the Japan Society for the Promotion of Science (JSPS) and the Supported Programs for the Strategic Research Foundation at Private Universities (No. S1411028) from the Ministry of Education, Culture, Sports, Science and Technology (MEXT) of Japan.

## APPENDIX

### A. ESTIMATIONS OF $E_{B-V}$ AND DISTANCE OF V5669 SGR

We estimated  $E_{B-V}$  of V5669 Sgr using the following three methods: (1) the intrinsic color index at the maximum of classical novae given by [van den Bergh & Younger \(1987\)](#); (2) the relation between  $W$ s of the diffuse interstellar band (DIB) and the interstellar hydrogen column density as practiced for V407 Lup ([Izzo et al. 2018](#)); and (3) the relation between  $E_{B-V}$  and  $W$ s of the DIB  $\lambda 6613.6$  among classical novae ([Munari 2014](#)).

The intrinsic color index at the maximum of classical novae is known to be  $(B-V)_{\max} = 0.23 \pm 0.06$  ([van den Bergh & Younger 1987](#)). Then, we obtain the intrinsic extinction  $E_{B-V}$  from the observed color index at the maximum,  $(B-V)_{\text{obs}} = 0.793 \pm 0.001$  (SMARTS Nova ATLAS), and hence,  $E_{B-V} = 0.56 \pm 0.06$ .

Furthermore, we estimate  $E_{B-V}$  of V5669 Sgr using DIBs, adopting the same procedure used for V407 Lup in [Izzo et al. \(2018\)](#). DIBs, and interstellar atomic absorption lines (IS) are also useful for estimating interstellar extinction. DIBs ( $\lambda 5705.1$ ,  $\lambda 5780.5$ ,  $\lambda 5797.1$ ,  $\lambda 6196.0$ , and  $\lambda 6613.6$ ) and IS (Na I D<sub>1</sub> D<sub>2</sub>, Ca II H K, Ti II  $\lambda 3242$ , and Ti II  $\lambda 3383$ ) are detected in our data on +24 and +28 d, because major components of IS of Na I D<sub>1</sub> D<sub>2</sub> and Ca II H K are heavily saturated, and DIB  $\lambda 5797$  and  $\lambda 6196$  are blended with other unidentified absorption lines in our spectra. We used two DIBs at  $\lambda 6614$  and  $\lambda 5780.5$  to estimate the extinction of V5669 Sgr. Measurable DIBs and IS are listed in Table 7. The correlation coefficients between the hydrogen column density of interstellar gas ( $N_{\text{H}}$ ) and these DIBs are given in Table 2 of [Friedman et al. \(2011\)](#). The averaged value of  $N(\text{H}) = 2.06 \pm 0.26 \times 10^{21} \text{ cm}^{-2}$ , affording  $E_{B-V} = 0.36 \pm 0.05$ , where we adopt the general value for the interstellar hydrogen total column density of  $N(\text{H})/E_{B-V} = 5.87 \times 10^{21} \text{ cm}^{-2} \text{ mag}^{-1}$  ([Bohlin et al. 1978](#)). Both  $W$ s of DIBs and IS Ti II of V5669 Sgr, which depend on the amount of IS should be larger than those of the V407 Lup ([Izzo et al. 2015](#)). Since we can only measure two DIBs, we use  $W$ s of Ti II  $\lambda 3242$  and  $\lambda 3383$  listed in Table 7 for our  $E_{B-V}$  estimation. Both  $W$ s of these Ti II lines and two DIBs in V5669 Sgr are larger than those in V407 Lup ( $W = 101.0 \pm 5.8 \text{ \AA}$  and  $W = 152.1 \pm 6.2 \text{ \AA}$  for Ti II  $\lambda 3242$  and Ti II  $\lambda 3383$ , respectively; [Izzo et al. 2018](#)).

[Munari \(2014\)](#) reported the empirical relation between  $E_{B-V}$  and  $W$ s of DIB  $\lambda 6614$  ( $W_{\lambda 6614}$ ),  $E_{B-V} = 4.40 \times W_{\lambda 6614}$ . Adopting this relationship for measuring the measured  $W$  of DIB  $\lambda 6614$  in V5669 Sgr, we obtain  $E_{B-V} = 0.41 \pm 0.01$ . The  $E_{B-V}$  estimated from DIBs  $\lambda 6614$  agrees with their standard deviations.

**Table 7.** List of Measured DIB and IS lines.

DIB/IS	$W$ (+24d) mÅ	$W$ (+28d) mÅ	$\log N(\text{H})$ $\times 10^{21} \text{cm}^{-2}$
Ti II 3242	$175.2 \pm 1.4$	$134.8 \pm 1.2$	
Ti II 3383	$234.0 \pm 1.4$	$227.5 \pm 1.4$	
DIB 5780.5	$338.3 \pm 3.5$	$338.3 \pm 3.5$	$2.62 \pm 0.56$
DIB 6613.6	$91.7 \pm 2.5$	$90.4 \pm 2.6$	$1.62 \pm 0.22$

Finally, we obtained the average of extinction,  $E_{B-V} = 0.44 \pm 0.03$ , from the above three values. The absolute magnitudes of V5669 Sgr are estimated through the the maximum-magnitudes and rate-of-decline (MMRD) relation (e.g. della Valle & Livio 1995; Downes & Duerbeck 2000; Özdönmez et al. 2018). Then, we obtained the distance to the nova using the above  $E_{B-V}$ . We used the latest MMRD formulation for Fe II novae, suggested in Özdönmez et al. (2018) with  $t_2$ , and obtained  $M_V = -7.8 \pm 0.4$ . Consequently, we identified the distance,  $d = 10.0 \pm 1.9$  kpc using the averaged  $E_{B-V}$  with the assumption of  $R_V = A_V/E_{B-V} = 3.1$ . These results are shown in Table 1.

## REFERENCES

- Althaus, L. G., Córscico, A. H., Isern, J., & García-Berro, E. 2010, *A&A Rv*, 18, 471
- Arai, A., Kawakita, H., Shinnaka, Y., & Tajitsu, A. 2016, *ApJ*, 830, 30
- Arnould, M., & Norgaard, H. 1975, *A&A*, 42, 55
- Asplund, M., Grevesse, N., Sauval, A. J., & Scott, P. 2009, *ARA&A*, 47, 481
- Barnsley, R. M., Smith, R. J., & Steele, I. A. 2012, *Astronomische Nachrichten*, 333, 101
- Boggess, A., Carr, F. A., Evans, D. C., et al. 1978, *Nature*, 275, 372
- Bohlin, R. C., Savage, B. D., & Drake, J. F. 1978, *ApJ*, 224, 132
- Cameron, A. G. W., & Fowler, W. A. 1971, *ApJ*, 164, 111
- Cescutti, G., & Molaro, P. 2019, *MNRAS*, 482, 4372
- Chambers, K. C., Magnier, E. A., Metcalfe, N., et al. 2016, arXiv e-prints, arXiv:1612.05560
- Chochol, D., Shugarov, S., Katysheva, N., & Volkov, I. 2015, in *The Golden Age of Cataclysmic Variables and Related Objects - III (Golden2015)*, 56
- della Valle, M., & Livio, M. 1995, *ApJ*, 452, 704
- Downes, R. A., & Duerbeck, H. W. 2000, *AJ*, 120, 2007
- Friedman, S. D., York, D. G., McCall, B. J., et al. 2011, *ApJ*, 727, 33
- Fujii, M. 2015, *IAUC*, 9277, 3
- Hachisu, I., & Kato, M. 2019, *ApJS*, 242, 18
- Hernanz, M., Jose, J., Coc, A., & Isern, J. 1996, *ApJL*, 465, L27
- Izzo, L., Della Valle, M., Mason, E., et al. 2015, *ApJL*, 808, L14
- Izzo, L., Molaro, P., Bonifacio, P., et al. 2018, *MNRAS*, 478, 1601
- José, J., & Hernanz, M. 1998, *ApJ*, 494, 680
- José, J., Shore, S. N., & Casanova, J. 2020, *A&A*, 634, A5
- Kato, M., Hachisu, I., & Cassatella, A. 2009, *ApJ*, 704, 1676
- Kramida, A., Yu. Ralchenko, Reader, J., & and NIST ASD Team. 2019, NIST Atomic Spectra Database (ver. 5.7.1), [Online]. Available: <https://physics.nist.gov/asd> [2016, January 31]. National Institute of Standards and Technology, Gaithersburg, MD., ,
- Molaro, P., Izzo, L., Bonifacio, P., et al. 2020, *MNRAS*, 492, 4975
- Molaro, P., Izzo, L., Mason, E., Bonifacio, P., & Della Valle, M. 2016, *MNRAS*, 463, L117
- Moore, C. E. 1972, A multiplet table of astrophysical interest - Pt.1: Table of multiplets - Pt.2: Finding list of all lines in the table of multiplets
- Munari, U. 2014, *Astronomical Society of the Pacific Conference Series*, Vol. 490, On some Aspects of Optical Observations of Novae, ed. P. A. Woudt & V. A. R. M. Ribeiro, 183
- Nakano, S., Itagaki, K., Kazarovets, E., & Samus, N. 2015, *IAUC*, 9277, 1
- Nilsson, H., Ljung, G., Lundberg, H., & Nielsen, K. E. 2006, *A&A*, 445, 1165
- Noguchi, K., Aoki, W., Kawanomoto, S., et al. 2002, *PASJ*, 54, 855
- Özdönmez, A., Ege, E., Güver, T., & Ak, T. 2018, *MNRAS*, 476, 4162
- Paxton, B., Bildsten, L., Dotter, A., et al. 2011, *ApJS*, 192, 3
- Prantzos, N. 2012, *A&A*, 542, A67
- Rukeya, R., Lü, G., Wang, Z., & Zhu, C. 2017, *PASP*, 129, 074201
- Selvelli, P., Molaro, P., & Izzo, L. 2018, *MNRAS*, 481, 2261
- Starrfield, S., Bose, M., Iliadis, C., et al. 2020, *ApJ*, 895, 70
- Starrfield, S., Truran, J. W., Sparks, W. M., & Arnould, M. 1978, *ApJ*, 222, 600
- Tajitsu, A., Aoki, W., Kawanomoto, S., & Narita, N. 2010, *Publications of the National Astronomical Observatory of Japan*, 13, 1
- Tajitsu, A., Sadakane, K., Naito, H., Arai, A., & Aoki, W. 2015, *Nature*, 518, 381
- Tajitsu, A., Sadakane, K., Naito, H., et al. 2016, *ApJ*, 818, 191
- van den Bergh, S., & Younger, P. F. 1987, *A&AS*, 70, 125
- Walter, F. M., Battisti, A., Towers, S. E., Bond, H. E., & Stringfellow, G. S. 2012, *PASP*, 124, 1057
- Wenger, M., Ochsenbein, F., Egret, D., et al. 2000, *A&AS*, 143, 9
- Williams, R., Mason, E., Della Valle, M., & Ederoclite, A. 2008, *ApJ*, 685, 451
- Williams, R. E. 1992, *AJ*, 104, 725

Williams, S. C., Darnley, M. J., Bode, M. F., &  
Bode, M. F. 2015, The Astronomer's Telegram,  
8101, 1

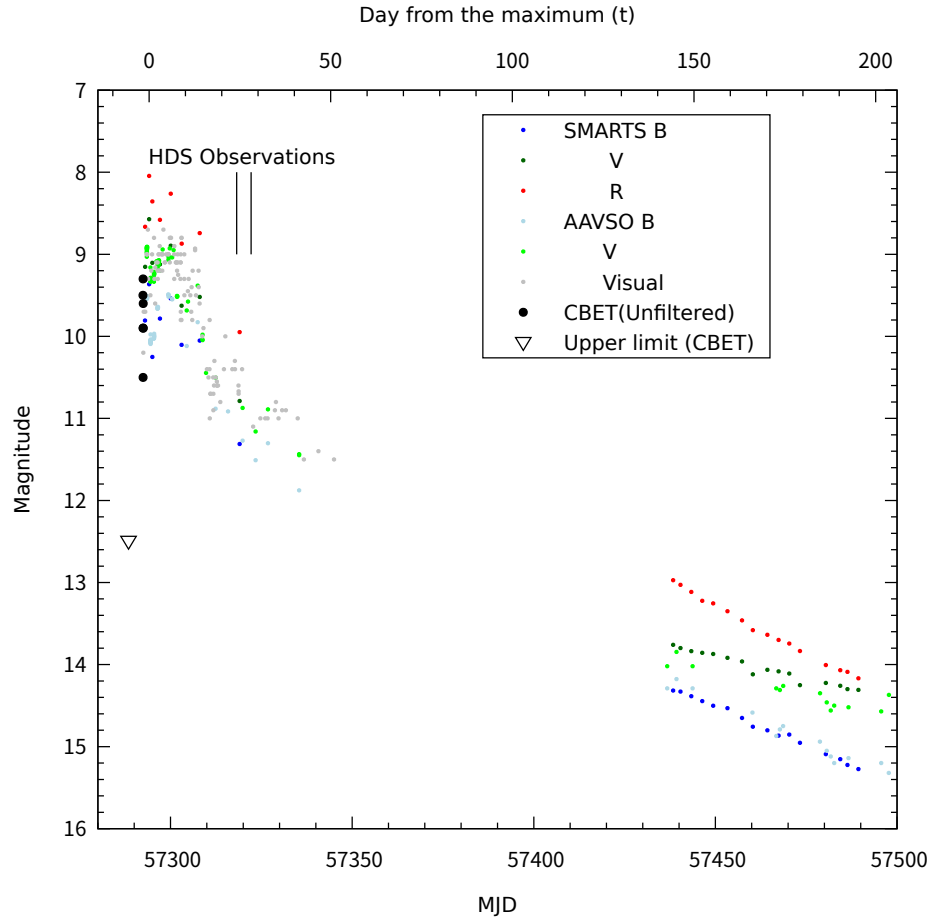


**Figure 1.** Light curves of V5669 Sgr. Photometric data were quoted from Nakano et al. (2015, CBET), the AAVSO Archives, and the Stony Brook/SMARTS Atlas. Vertical lines denote the time of our observations on +24 and +28 d.



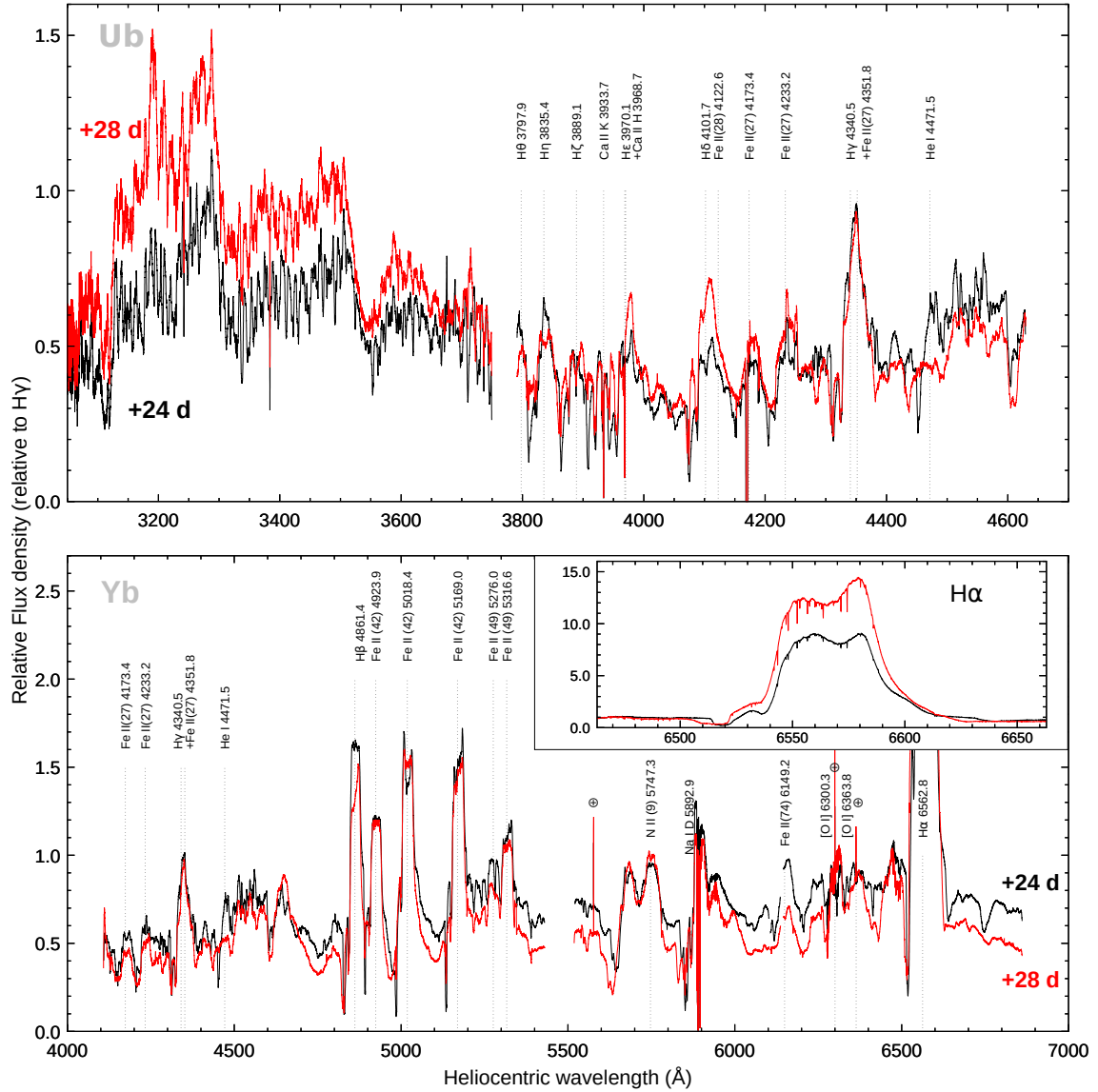


**Figure 2.** Overall spectra of V5669 Sgr on +24 d (black) and +28 d (red). The upper and lower panel show “Ub” region spectra (3050–4631  $\text{\AA}$ ), and “Yb”-setting spectra (4108–6865  $\text{\AA}$ ), respectively. The vertical axis denotes the relative flux density normalized with the peak of emission components of H $\gamma$  included in both regions. Dotted lines show the line identifications of strong emission lines. Crossed circles indicate the telluric emission lines. The magnified view in H $\alpha$  is shown in the inset in the lower panel.

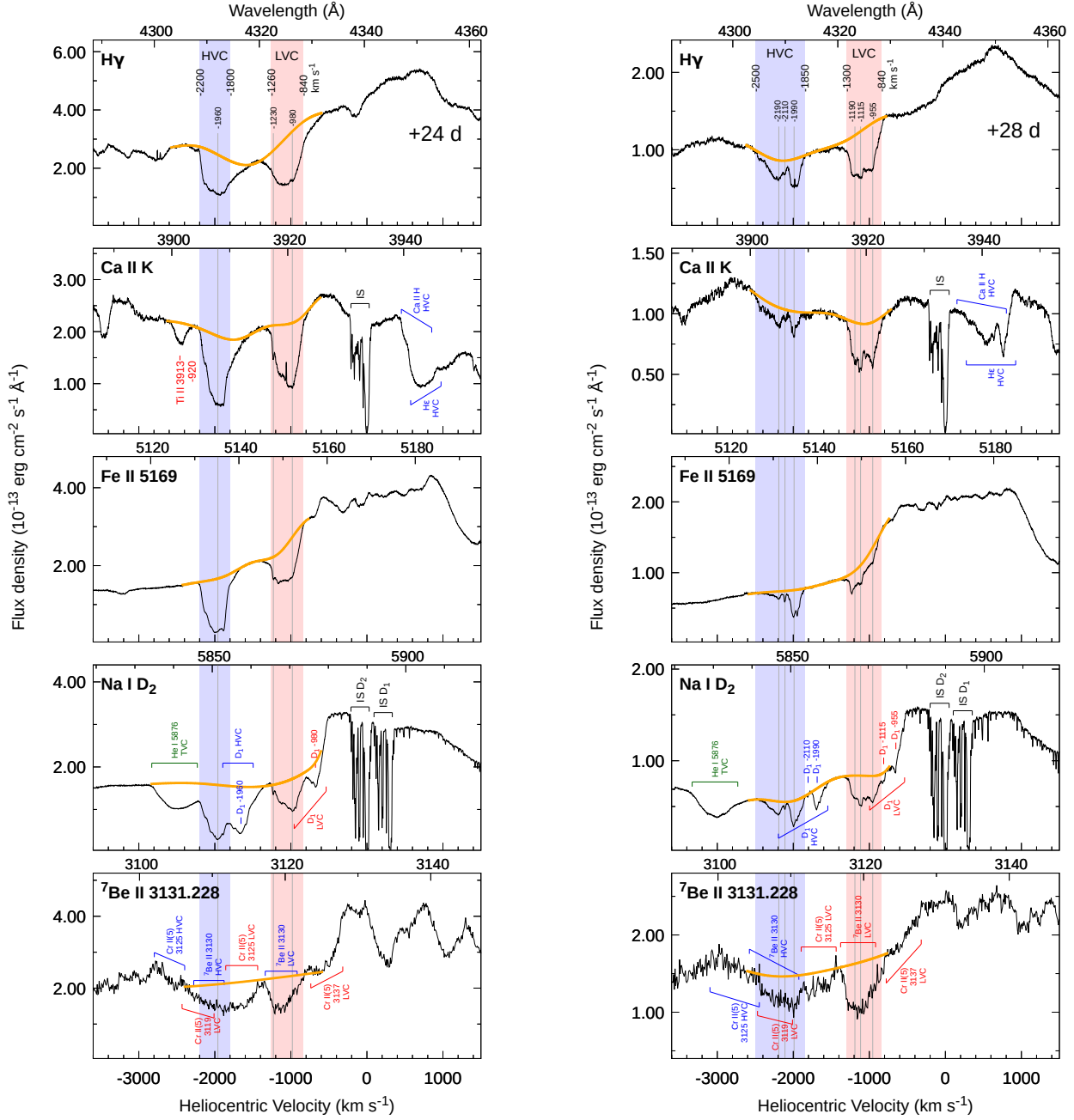


**Figure 3.** Velocity components in the major lines ( $H\gamma$ , Ca II K,  ${}^7\text{Be II Na I D}_2$ , and Fe II  $\lambda 5169.028$ ) on +24 d (left) and +28 d (right). Orange curves indicate continuum fitting curves for these lines. Red and blue shaded regions indicate ranges of the LVC and HVC, respectively. Gray vertical lines are subcomponents in these absorption systems determined from  $H\gamma$ , Fe II  $\lambda 5196.028$ , and Ca II K.

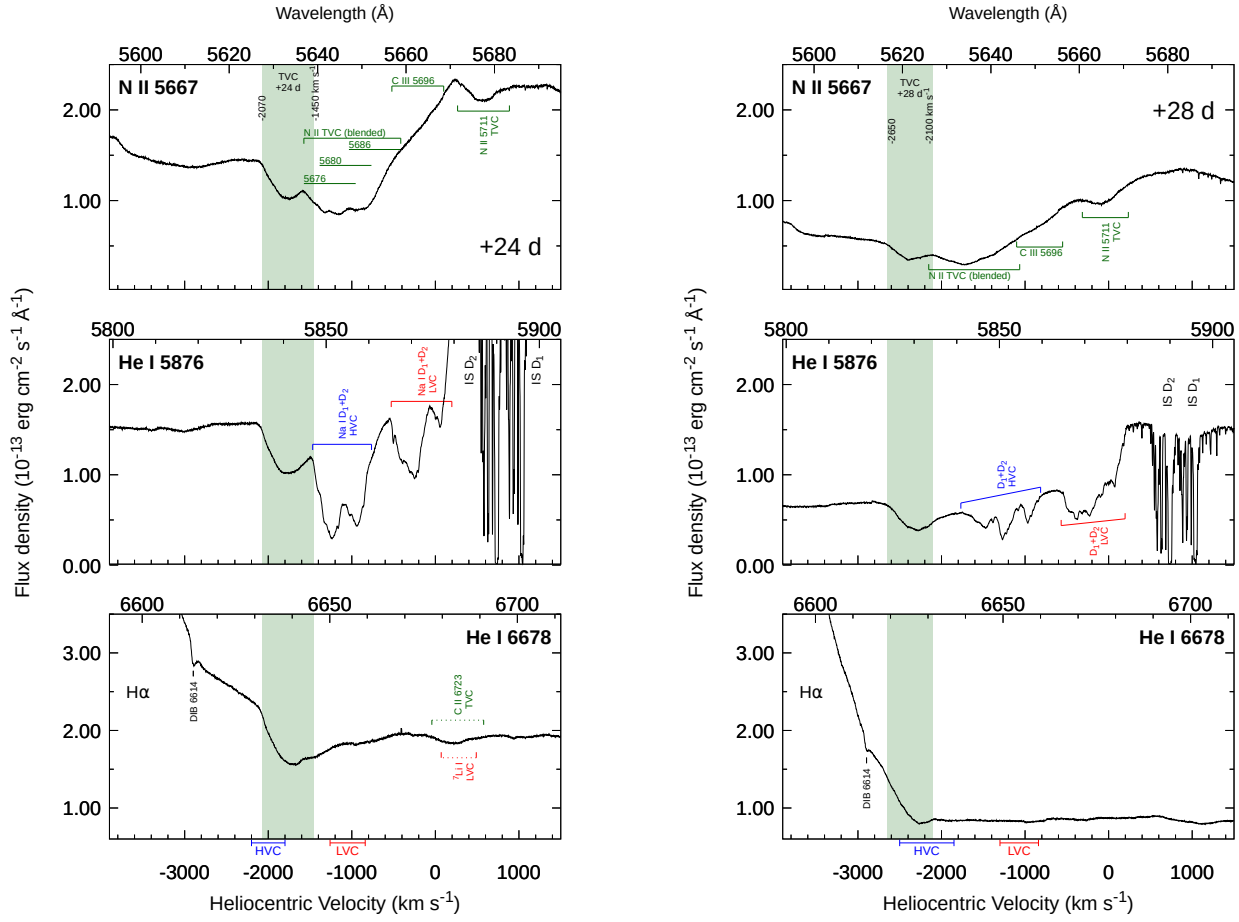


**Figure 4.** Temporal developments of the absorption component in the TVC (N II  $\lambda$ 5666.63, He I  $\lambda$ 5875.621,  $\lambda$ 6678.151). The left and right panels correspond to those on +24 and +28 d, respectively. The green shaded regions denote the velocity ranges of the TVC (Section 4.3) for these lines. Green horizontal lines with labels indicate expected positions of the TVC originating from other lines. Red and blue ones are LVC and HVC for other lines, respectively. The horizontal red and blue lines below the bottom axis show the velocity ranges of LVC and HVC on both epochs, respectively.

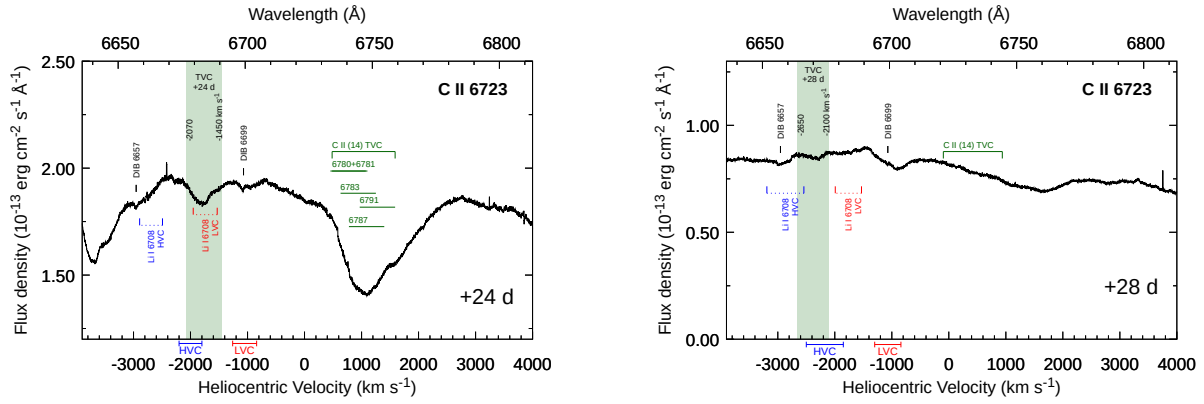


**Figure 5.** Same as Figure 4, but for the region of C II  $\lambda 6723.32 \text{ \AA}$  on +24 and +28 d.

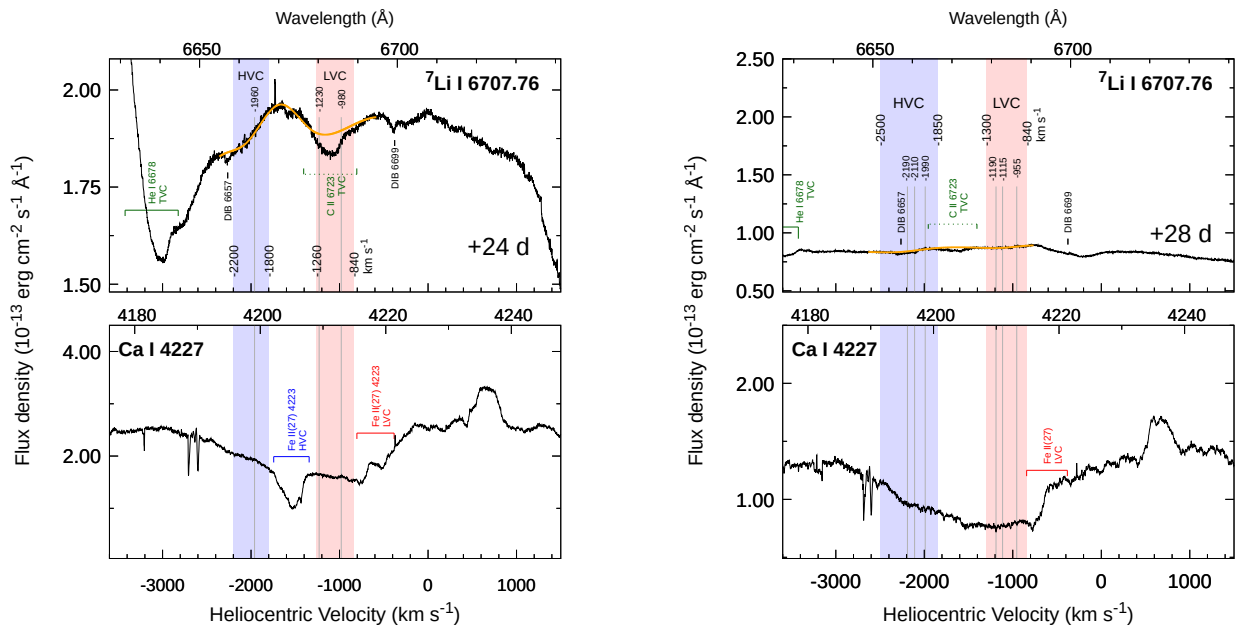


**Figure 6.** Same as Figure 3, but for regions of Ca I  $\lambda 4226.73$  and Li I  $\lambda \lambda 6707.76$ . No significant absorption components of Ca I  $\lambda 4226.73$  are present.

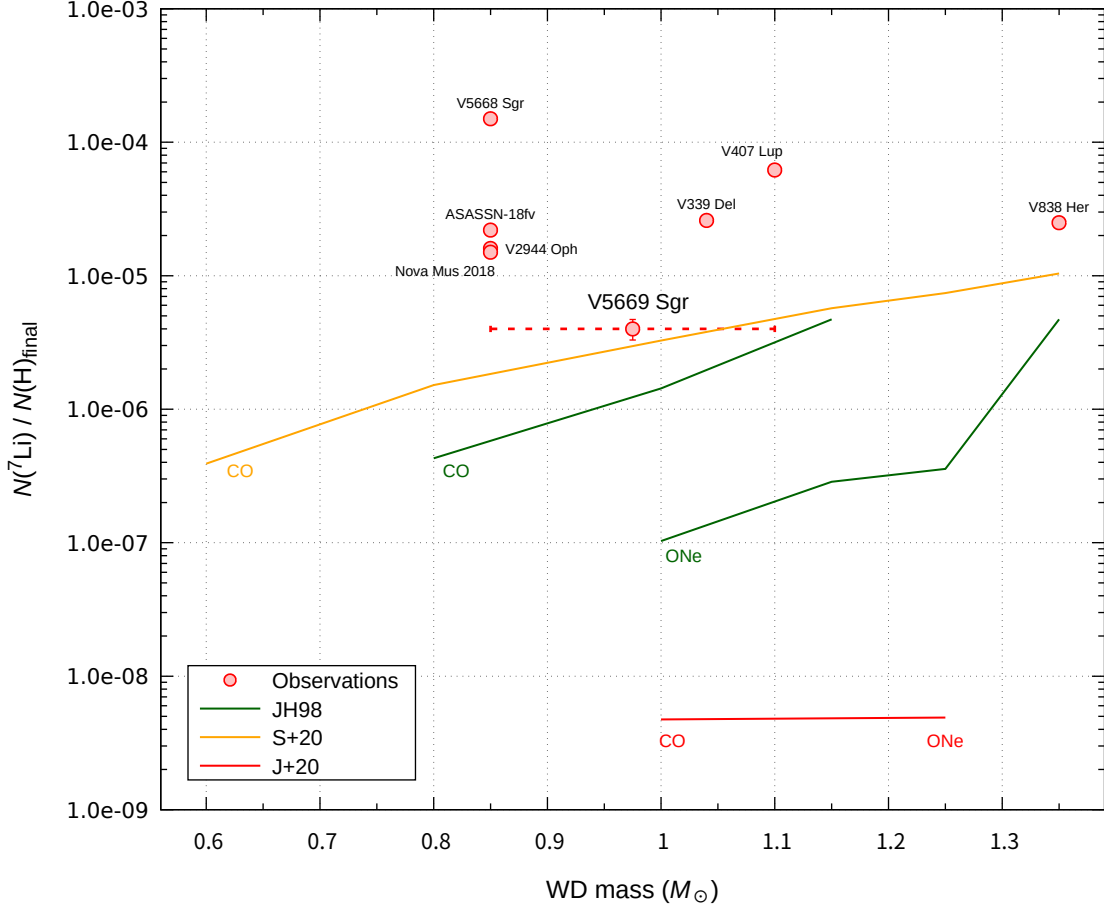


**Figure 7.** Comparison with observed Li abundances and recent numerical simulations along with WD masses. Red bordered circles denote averages of observed abundances listed in Table 6. The dotted horizontal line with the value of V5669 Sgr shows the considerable WD mass range of V5669 Sgr. Note that WD masses for all observed novae, which have been estimated from the duration of their light curves, generally have similar large error bars. Since evaluating errors for each WD mass estimation is difficult, we simply plotted middle points of each estimated mass ranges for each observed nova. The green, orange, and red lines correspond to theoretical predictions; highest values for each WD mass in José & Hernanz (1998, JH98), the 25%–50% mixing model for only CO novae of Starrfield et al. (2020, S+20) and ‘123–321 models’ of José et al. (2020, J+20), respectively.